Citation &
Copyright (to be inserted by the publisher)

A unified approach to digital photoelasticity incorporating image filtering and inverse methods

I. A. Jones[1], P. Wang[1], A. A. Becker[1], T. H. Hyde[1],
T. P. Pridmore[2] and A. H. Ghali[2]

[1] School of MMMEM, University of Nottingham, University Park, Nottingham NG7 2RD, UK

[2]Computer Science and IT, University of Nottingham, Jubilee Campus, Nottingham NG8 1BB, UK

Keywords: Photoelasticity, boundary elements, inverse methods, phase stepping, hybrid methods

Abstract. A unified, hybrid experimental/numerical approach to digital photoelasticity has been developed. The system consists of an automated polariscope with image capture facilities together with a suite of dedicated software for setting up and controlling the polariscope, for extracting and unwrapping the isoclinic and isochromatic data, for constructing a boundary element (BE) model congruent with the edges of the specimen on the photoelastic images, and for obtaining separated stresses and boundary conditions such as contact stresses via an inverse BE technique. In this paper, the integration of the various techniques is described and illustrated using typical results.

Introduction

The present project is centred around a hybrid stress analysis method combining phase-stepping photoelasticity with a numerical approach consisting of an inverse boundary element method, but also involves a number of new and extended experimental and analytical techniques. The aim of this paper is to present and illustrate the complete picture of how the system fits together, rather than to duplicate existing descriptions and evaluations of the individual components of the system.

The approach described here is just one example of a "hybrid" stress analysis technique in that it combines experimental and numerical (boundary element) stress analysis. The concept of hybrid methods dates back at least to 1981 [1]. An overview of the area was given by Kobayashi [2] in 1993. Since then, interest in hybrid approaches has gained considerable momentum. Rowlands and his co-workers have developed the concept by combining a variety of experimental and numerical approaches; some examples are reviewed in reference [3], but none of these involve photoelasticity.

The present authors [4] have already reviewed some of the literature on hybrid methods involving the boundary element method (BEM). Since that review was undertaken, Laermann [5] has presented a hybrid approach applied to a variety of three-dimensional and viscoelastic problems. Of particular interest is his example in which photoelastic data from the edge (but not the interior) of a specimen are used in constructing a boundary element solution to the Laplace equation $\nabla^2(\sigma_1+\sigma_2)=0$ to the boundary conditions then solving the resulting $(\sigma_1+\sigma_2)$ field simultaneously with the isochromatic data representing $(\sigma_1-\sigma_2)$ in order to separate the stresses. Broadly similar approaches are also described elsewhere [6,7]. The present approach therefore appears to be unique in using data from within a photoelastic specimen in conjunction with an inverse BE approach.

The approach described here would be impractical without the automation of the photoelasticity process via digital imaging and phase-stepping, and much has been written in recent years on these and other automated approaches to photoelasticity. Good overviews have been presented [8,9] and new phase-stepping algorithms have continued to be published (e.g.[10]). A detailed literature review will not be undertaken here. Instead, an emphasis will be placed on the overall architecture of the photoelasticity system developed at Nottingham, developments made on each of the aspects of the system will be summarised, and the application of the system will be illustrated via typical results.

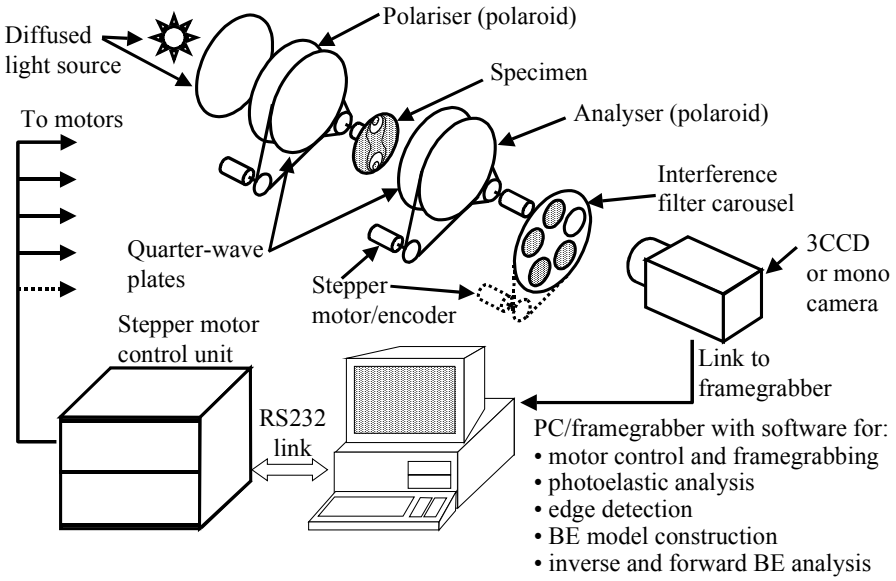

Figure 1: diagram showing hardware and software involved in photoelasticity system

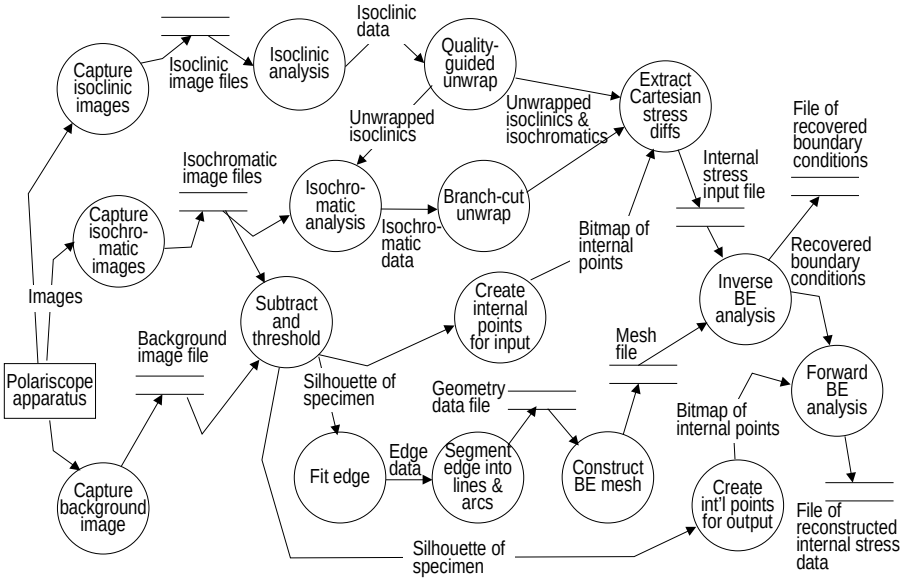

Figure 2: data flow diagram showing data and processes involved in photoelasticity system

Overview of system

The system is summarized by the apparatus diagram in Fig. 1 and the dataflow diagram in Fig. 2 showing the main processes and data items. The starting points for the analysis are:

(a) A set of images captured for determination of isoclinic data

(b) A set of images captured for determination of isochromatic data

(c) A background image against which one of the above images can be compared.

Fringe maps defining the isoclinic and isochromatic data are obtained from the captured images. Unwrapping processes are necessary to place the isoclinic angle in the correct quadrant, and to ensure that the isochromatic data correctly identify both the integer and fractional part of the relative retardation (fringe order). The unwrapped isoclinic and isochromatic data are then used to obtain values of $\sigma_{xx}-\sigma_{yy}$ and σ_{xy} at numerous internal points (selected as described later) for input to the boundary element model. This model will have been constructed as follows. A typical image of the

specimen from the dataset described earlier is compared via differencing and thresholding techniques with an image of the empty polariscope (i.e. omitting the specimen) captured using identical lighting conditions and polariscope setting. The resulting silhouette is then used in conjunction with edge detection and edge segmentation algorithms (and, currently, with some user interaction) to segment the boundary into arcs and lines upon which the boundary element model is based. The silhouette is also used as the basis for selecting the locations of the internal points to be used for the boundary element input. An inverse boundary element analysis is then performed, in which the boundary conditions are found from the internal stress data (inverting the usual process where internal stress data are found from the boundary conditions). Separated stresses can then be found at specified internal points by performing a conventional ("forward") boundary element analysis. By this means, datasets corresponding to the photoelastic input data can be reconstructed from the separated stresses and compared with the experimentally-obtained isoclinics and isochromatics in order to confirm that the inverse analysis is valid. Having described the overall process, it is instructive to examine each aspect of the system in order to understand how the different aspects fit together.

Apparatus and phase-stepping algorithm

The apparatus used (Fig. 1) is an enhancement of that described in reference [11]. All four optical elements (polariser, analyser and both quarter wave plates) are driven by stepper motors in closed-loop mode under the control of a McLennan stepper motor controller and driver system. Additionally a fifth stepper motor is provided for rotating a carousel containing four narrow-bandwidth (10nm) interference filters (and one free space) to allow monochromatic light of different colours to be used for analysis rather than relying upon the camera's internal filters, though the automation of this feature has not yet been implemented. The flexibility of this system allows sequences of images to be captured for almost any kind of transmission photoelasticity approach, such as those of Patterson [12] or Hecker and Morsche [13]. However, because of the potential for error sensitivity in the inverse boundary element method, considerable effort was put into exploring new approaches to digital imaging photoelasticity in order to minimise error in the results obtained. Phase-stepping was selected from the various methods in the literature. Here a least-squares approach is used in conjunction with an overdetermined experimental dataset of many images, rather than seeking to keep the number of images low as in many published strategies.

Phase-stepping photoelasticity may be regarded as an inverse method in its own right, since the aim is to invert the optical model of the polariscope and specimen in order to obtain the optical characteristics of the specimen (principal directions and relative retardation). Using the results of one inverse analysis (phase-stepping photoelasticity) as the input to another inverse analysis (the inverse BEM) introduces very serious scope for sensitivity to errors, and the present technique aims to minimise this by keeping to a minimum the number of unknowns to be found simultaneously within the analysis of the phase-stepping results. Rather than finding the isoclinic and isochromatic parameters simultaneously, a two-stage process is used which may be regarded as a generalisation of the approach of Hecker and Morsche [13]:

(a) A set of polarisation-stepped images is used to determine the isoclinic angle from the phase angle of the light intensity variation over the sequence of images. The isoclinic angles must be unwrapped (and may optionally be re-wrapped into an arbitrary 180° range) in order to distinguish correctly between the σ_1 and σ_2 directions.

(b) A further set of images is captured with the analyser and second quarter wave plate set to a circular polariser configuration, and with the polariser and first quarter wave plate set to cover a wide range of different polarisation states such as those defined by the vertices of a dodecahedron erected within the Poincaré sphere. With prior knowledge of the isoclinic angle, a least-squares fit to an optical model of the polariscope and specimen is used to determine the relative retardation.

This approach was described in some detail within reference [14] and is found in practice to give very clean maps of isoclinics and especially of isochromatics. As an example, a typical image from the isochromatic series for a frozen-stress gear specimen, and greyscale images of the isoclinic and isochromatic maps obtained, are shown in Figs. 3 (a-c)

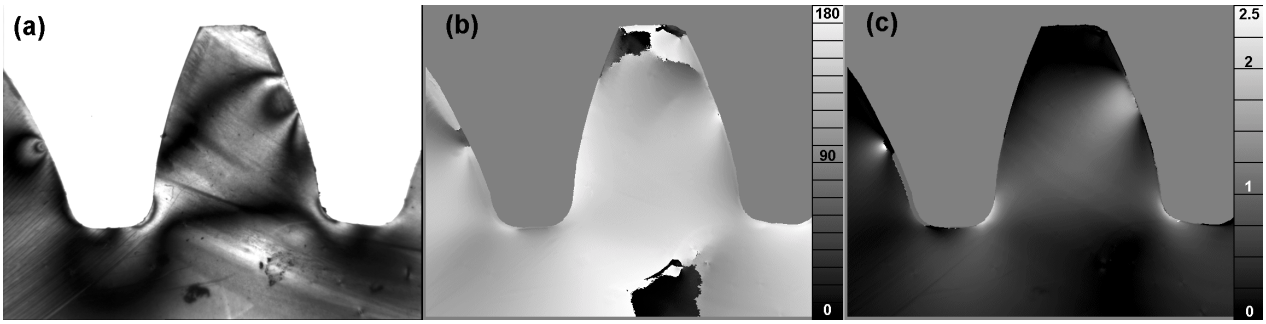

Figure 3: (a) Typical image from isochromatic sequence (green colour plane captured using JAI CV-M90 3CCD camera, mid-band wavelength 551 nm) (b) Isoclinic map (c) Isochromatic map

Unwrapping of isoclinic and isochromatic data.

Two approaches to the unwrapping of isoclinic and isochromatic fringes have been developed. The first is the use of the coefficient of multiple determination R^2 as a measure of the goodness-of-fit of the measured data to the assumed photoelastic behaviour, for use within a suitable quality-guided algorithm such as that presented by Ghiglia and Pritt [15]. This has proved to be better suited to the unwrapping of isoclinic data than of isochromatic data, for which Goldstein's branch-cut algorithm (also presented in [15]) has been found to give more reliable results. The second is a method known as fringe combination matching [16], in which the values of fractional fringe order measured on the red, green and blue channels are matched to a unique value of complete fringe order. This is a new variant on the existing approach known as RGB photoelasticity [17]. This makes it possible to distinguish between fringe values with the same fractional part but different integer parts. The fringe combination matching method is well suited to the automatic identification of the "seed point" value for initiating a more direct unwrapping approach such as the quality-guided unwrapping; it also represents one of very few examples of the integration of RGB and phase-stepping photoelasticity methods. Recent work [18] has extended the fringe combination matching approach to cover more difficult situations such as where the σ_1 and σ_2 directions have been incorrectly identified due to incorrect unwrapping of the isoclinics, and where results are presented so that they are "wrapped" so as to preserve continuity of fringe value but not of fringe gradient.

Edge detection on translucent specimens against imperfect backgrounds

Techniques have been developed for extracting boundary element models from colour images of translucent objects captured within the polariscope. An image is acquired either under traditional lighting conditions or by configuring the polariscope to provide a "light field" background against which the specimen will give reasonable contrast (some of the images used for finding the isochromatics are acceptable for this purpose. A corresponding image omitting the specimen is also captured. Such images typically contain extraneous components of the polariscope or supports for the specimen. These are detected and removed by a combination of image differencing, thresholding and filtering. The latter is required to eliminate noise arising mainly from poor contrast between specimen background image. The resulting silhouette is used for three purposes:

(a) As a mask for use within the unwrapping processes described above, in order to limit the unwrapping to the specimen region rather than spilling off into the background region.

(b) As a template for the manual or automatic choice of the internal points at which the photoelastic data are evaluated for use within the inverse BE model

(c) For use in finding the boundary of the specimen via a segmentation process

The boundary is itself segmented to produce a representation in terms of simple geometric primitives (lines and arcs). This is a difficult problem since the input curve typically contains subtle curvature discontinuities that must be located to a high degree of accuracy, and some manual intervention is currently required to overcome any ambiguities. The boundary element model is then constructed from these geometric primitives. More details of the algorithms are given in reference [19], and examples of some of the images involved are shown in Fig. 4.

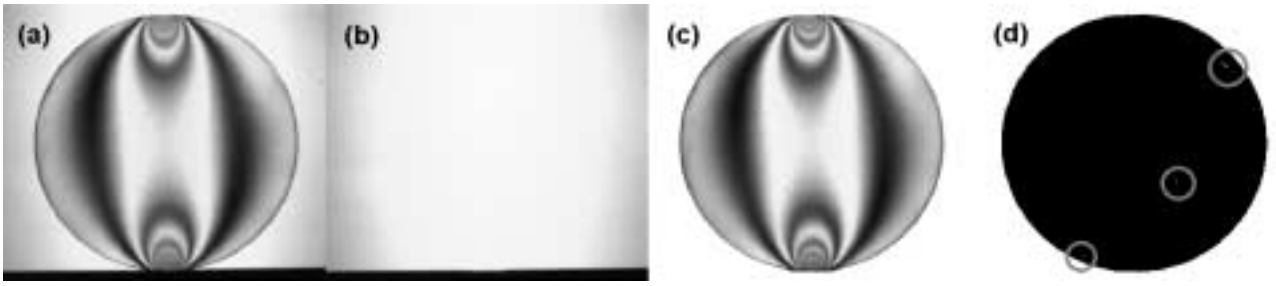

Figure 4 (a) Typical image from isochromatic series (b) corresponding image omitting specimen (c) result of differencing and thresholding (d) result of further thresholding to obtain silhouette. Localised noise (barely visible, circled) is removed by logical filtering prior to edge detection.

Object-oriented Inverse Boundary Element Technique

As indicated earlier, this forms the core of the system and various aspects of its development and testing have already been described in some detail in earlier publications. The present paper presents only a brief overview of the technique and its object-oriented implementation in C++.

The aim of the system is to recover the unknown tractions and displacements around the boundary of the specimen, and hence to reconstruct the individual (separated) stresses at all points within and on the surface of the specimen. The theoretical starting point for this analysis is the forward BE formulation, which is presented in many textbooks including that by Becker [20], and is based upon two boundary integral equations. The surface integral equation expresses the displacement components at an arbitrary point p at or within the boundary Γ of the object in terms of boundary integrals involving all surface displacements u and tractions t:

$$u_i(p) + \int_\Gamma T_{ij}(p,Q)u_j(Q)d\Gamma(Q) = \int_\Gamma U_{ij}(p,Q)t_j(Q)d\Gamma(Q) \qquad (1)$$

where U_{ij} and T_{ij} are called the "surface" displacement and traction kernels, respectively, and are functions of the coordinates and material properties, but not the boundary conditions, and point Q is an arbitrary point on the boundary. The interior integral equation is of similar form and expresses the stress state (at an arbitrary internal point p in terms of integrals around the boundary Γ involving the displacements u and tractions t and expressed in terms of so-called "interior" kernels.

In the BEM, the boundary Γ is discretised into elements. In a conventional (forward) BE analysis the boundary conditions at any given node will take the form of known displacements or known tractions. The discretised form of Eq. 1 is used (after rearrangement) to obtain the complete set of displacements and tractions at every node, and the stress vector $\{\sigma\}\equiv[\sigma_{xx}(p), \sigma_{yy}(p), \sigma_{xy}(p)]^T$ at any internal point may then be calculated from a discretised form of the interior integral equation:

$$\{\sigma\} = [D]\{t\} - [S]\{u\}. \qquad (2)$$

At first sight, it would seem possible to rearrange and invert Eq. 2 to yield the set of unknown tractions and displacements in terms of the the internal stresses $\{\sigma\}$. However, it has been demonstrated [4] that inverse methods relying on the interior kernels only cannot be used to obtain the solution, and it is necessary also to make use of the surface integral equation (Eq. 1). Moreover, some of the boundary conditions are already known and need to be taken into account:

(a) On some parts of the boundary (termed Γ_{bc}) the boundary conditions are prescribed, i.e. either the tractions or the displacements are given, so the unknowns on this region are either the displacement or the traction but not both. $\{x_{bc}\}$ is used to denote the mixed unknowns in this region.

(b) On the remainder of the boundary (termed region Γ_0), notably contact regions and regions where the domain has been cropped, both the displacements $\{u_0\}$ and tractions $\{t_0\}$ are unknown.

The discretised surface integral equation is used to eliminate the unknown tractions $\{t_0\}$ from boundary region Γ_o and mixed unknowns $\{x_{bc}\}$ from the prescribed boundary Γ_{bc}. Rearrangement [21, 22] yields an equation with the displacements $\{u_0\}$ in the region Γ_0 as the only unknowns:

$$[H_0]\{u_0\} = \{\sigma\} + \{R_0\} \tag{3}$$

where $[H_0]$ and $\{R_0\}$ are respectively a matrix and a column vector, rearranged from the various matrices of integrated kernels and (in the case of $\{R_0\}$) from the known boundary values.

In practice, not all of the components of $\{\sigma\}$ are known individually. However, it is possible to replace $\{\sigma\}$ in the above analysis with $\{\Delta\sigma\}\equiv[(\sigma_{xx}(p)-\sigma_{yy}(p)), \sigma_{xy}(p)]^T$, which contains terms which are easily calculated from the unwrapped isoclinic angle θ and isochromatic data (proportional to $\sigma_1-\sigma_2$) using the well-known Mohr's circle equations. Matrices $[S]$ and $[D]$ are similarly rearranged to give new matrices $[\Delta S]$ and $[\Delta D]$. Eq. 2 therefore becomes:

$$\{\Delta\sigma\} = [\Delta D]\{t\} - [\Delta S]\{u\} \tag{4}$$

The approach described in Eqs 3 and 4 for Cartesian stress can then be used without further alteration to reconstruct the unknown boundary variables using the photoelastic data by replacing $[\sigma]$, $[S]$ and $[D\}$ with $[\Delta\sigma]$, $[\Delta S]$ and $[\Delta D]$, respectively.

Software to undertake this process has been written in C++ using an overall object-oriented architecture making use of inheritance. This enables the forward and inverse BE analyses to share a program structure [23] and to inherit data (attributes) and procedures (methods) common to both.

The above procedure requires $\{\Delta\sigma\}$ to be evaluated at a large number of internal points, which take the form of sampling positions for evaluating the photoelastic data. Two conflicting issues govern their placement: internal points cannot be placed too close to the boundary otherwise the integrals become singular, but Saint-Venant's principle implies that the points must not be placed too far from the boundary otherwise their influence on the boundary conditions becomes weak. In practice a compromise is required, and the distribution of sampling points is biased so that most of the points are placed close to but not immediately adjacent to the boundaries where unknown boundary conditions are to be determined. A typical inverse BE mesh and the corresponding set of internal points is shown in Fig. 5.

The final stage of the process is a forward BE analysis based upon the fitted boundary conditions to obtain the separated stresses at any desired internal position. It is possible to evaluate the separated stresses (and the principal stress directions) at each pixel position within the specimen and hence present the results in a format directly comparable with the input data (isochromatics and isoclinics), for example as shown in Fig. 6. It should be noted that unless interpolation is used (not undertaken here) the continuous area covered by the resulting map cannot extend quite to the boundary of the specimen since the internal points must not coincide with the boundary. Stresses are however evaluated at the nodes, though these points may not be clearly visible in the images.

Quantitative evaluations for this and other examples are presented in references [21] and [22] and further evaluations are ongoing. In particular, the system has successfully (and reasonably consistently) reconstructed the approximately Hertzian contact stress profiles occurring within the contact regions of the gear tooth and other contact examples.

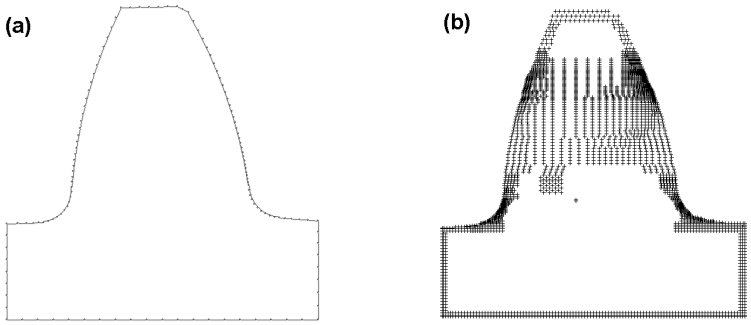

Figure 5: (a) Mesh used for inverse boundary analysis of gear tooth (b) Internal points used for sampling of photoelastic data (note: images not shown to same scale).

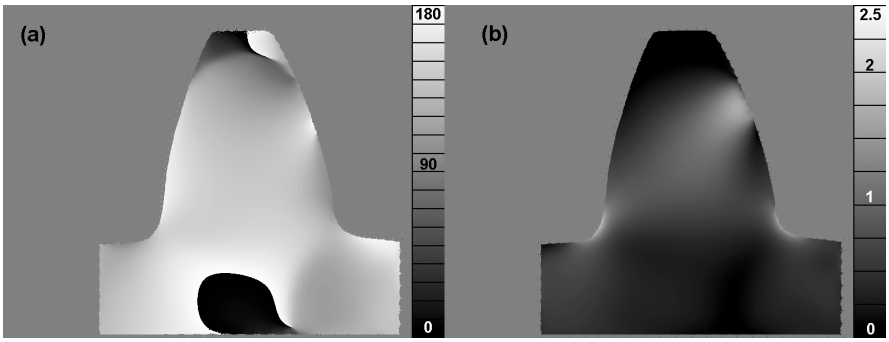

Figure 6: Images recreated from boundary element results: (a) Principal stress orientation and (b) principal stress difference expressed in units of fringe order. Compare with Figs. 3(b&c) respectively.

Discussion and conclusions

This paper has presented an overview of a successful research project which has not only drawn together a variety of previously separate experimental techniques but has also drawn photoelasticity and boundary element techniques together via a new hybrid method based upon inverse boundary element analysis. It has been demonstrated that the system is able to reconstruct the isoclinic and isochromatic maps which agree closely with the experimental data, and further results presented elsewhere suggest that the system is successful in reconstructing the boundary conditions in contact problems. The aim here has not been to present quantitative evaluations of the individual techniques or of the system; some of these have already been published while a more thorough investigation of the repeatability and behaviour of the complete system is ongoing.

Acknowledgements

The work upon which this publication is based was funded by the Engineering and Physical Sciences Research Council under grant GR/M40684/01, and was undertaken within the framework of the University Technology Centre in Gas Turbine Transmissions at Nottingham which is kindly supported by Rolls-Royce plc. The authors gratefully acknowledge the assistance in the manufacture and loading of the specimens given by Mr A.Higgins and Mr M. Foreman, and the assistance by Dr H. Jones in editing the manuscript. The contributions to the project of a number of undergraduate students and of Dr D. Chen also deserve recognition.

References

[1] K.H. Laermann: Exp. Mech., Vol 21 (1981), pp. 49–58.

[2] A.S. Kobayashi, in A.S. Kobayashi, ed. *Handbook on Experimental Mechanics*, 2nd ed, (Society for Experimental Mechanics, Bethel, CT, 1993), pp. 751-783.

[3] S.T. Lin and R.E. Rowlands: Optics and Lasers in Engineering Vol. 32 (1999), pp. 257–298

[4] D. Chen, A.A. Becker, I. A. Jones, T. H. Hyde and P. Wang: *J. Strain Analysis*, Vol. 36 (2001), pp. 253–264.

[5] K.-H. Laermann: Optics and Lasers in Engineering Vol. 32 (1999) pp. 183–203

[6] C. Umeagukwu: Int. J. of Mech. Eng. Edu., Vol. 17 (1989), pp. 163–174.

[7] Y. Mitsui, and S. Y. Yoshida: ASCE J. Eng. Mech., Vol.109 (1983),pp. 619–631.

[8] E.A. Patterson and Z.F. Wang: J. Strain Analysis, Vol. 33 (1998), pp. 1–15.

[9] K. Ramesh: *Digital Photoelasticity*. (Springer, Berlin, 2000).

[10] S. Barone, G. Burriesci and G. Petrucci: Exp. Mech., Vol. 42 (2002), pp. 132–139.

[11] A.A. Becker, P. Wang, and I.A. Jones: Paper 26 in *Proc. Soc. for Exp. Mechanics Conf.*, Milwaukee, Wisconsin, 10-12 June 2002

[12] E.A.Patterson, and Z.F. Wang: Strain, Vol. 27 (1991) pp. 49-56.

[13] F.W. Hecker and B. Morsche, in Weiringa, H (ed.): *Experimental Stress Analysis* (Nijhoff, The Netherlands, 1986), pp. 532-542.

]14] A. Triplow, I.A. Jones and D.L. Chen: *Proc. 4th Int. Conf. on Modern Practice in Stress and Vibration Analysis*, Nottingham, 5-7 September 2000, pp. 111-122.

[15] D C Ghiglia, and M.D. Pritt, *Two-dimensional phase unwrapping : theory, algorithms, and software*. New York: J. Wiley, 1998.

[16] I.A. Jones and P. Wang: Complete fringe order determination in digital photoelasticity using fringe combination matching, accepted for publication in *Strain.*

[17] A. Ajovalasit, S. Barone and G. Petrucci: Exp. Mech., Vol. 35 (1995), pp. 193-200.

[18] I.A. Jones: Paper 260 in in *Proc. Soc. for Exp. Mechanics Conf.*, Charlotte, North Carolina, 2-4 June 2003.

[19] A.Ghali, T.P. Pridmore, A. Jones, P. Wang and A. Becker, Proc. SPIE vol. 5016 paper 21 (presented at *Computational Imaging*, Santa Clara, 20-24 January 2003).

[20] A.A. Becker: *The boundary element method in engineering* (McGraw-Hill, UK, 1992).

[21] I.A. Jones, A. A. Becker and P. Wang: Paper 278 in *Proc. Soc. for Exp. Mechanics Conf.*, Charlotte, North Carolina, 2-4 June 2003.

[22] P. Wang, A.A. Becker, I.A.Jones and T.H. Hyde: Paper 16 in *Proc. 6th Int. Conf. on Engineering Computational Technology* (ECT-2002), Prague, 4-6 September 2002.

[23] I.A. Jones, A.A. Becker, P. Wang, D.L. Chen, and T.H. Hyde: Paper 13 in *Proc. 8th Int Conf on Civil & Structl Eng Comp*, Eisenstadt, Vienna, 19-21 Sept 2001.